Reaction of Hydroxyl Radical with Nitric Acid: Insights into Its Mechanism†

Steven S. Brown,*,‡ James B. Burkholder, Ranajit K. Talukdar,§ and A. R. Ravishankara§,||

NOAA Aeronomy Laboratory, R/AL2, 325 Broadway, Boulder, Colorado 80305

Received: July 5, 2000; In Final Form: October 17, 2000

The rate constant for the reaction of hydroxyl radicals with nitric acid has an unusual pressure and temperature dependence. To explore the mechanism for this reaction, we have measured rate constants for reactions of isotopically substituted species OD + DNO_3, OH + DNO_3, OD + HNO_3, and ^{18}OH + HNO_3 and the yield of NO_3 product. Deuterium substitution on nitric acid results in more than a 10-fold reduction in the rate constant, removes the pressure dependence (over the observed range of 20−200 Torr in He and SF_6), and leads to a strongly curved Arrhenius temperature dependence. Deuterium substitution on hydroxyl increases the rate constant slightly but does not change the pressure dependence. There is no evidence for exchange reactions in the isotopically mixed reactions. Absorption measurements of the NO_3 product yield show that the title reaction produces nitrate radical with unit efficiency over all temperatures and pressures studied. We discuss the implications of the measured rate constants, product yields, and lack of isotopic exchange in terms of a mechanism that involves formation of a hydroxyl radical−nitric acid complex and its subsequent reaction to give NO_3 and H_2O.

I. Introduction

Nitric acid is the most abundant reactive nitrogen species in the atmosphere, and it is a reservoir for NO_x (defined as the sum of NO and NO_2), which plays many critical roles in the troposphere and stratosphere. The reaction of HNO_3 with OH is a significant pathway for regenerating NO_x from this reservoir.

$$OH + HNO_3 \rightarrow H_2O + NO_3 \qquad (1)$$

We recently reported the value of k_1, the rate constant for this reaction, between 200 and 375 K in 10−500 Torr of four different buffer gases (He, N_2, O_2, and SF_6).[1] Our values were significantly larger at low temperature than the previous recommendation for atmospheric modeling.[2] Our larger values of k_1 have a significant impact on calculated atmospheric partitioning between NO_x and NO_y [3] (defined as all oxidized nitrogen species other than N_2O), as well as on modeled ozone destruction rates by different chemical families (i.e., HO_x, ClO_x, etc.).[4,5] One of the reasons for the difference between our values and previous recommendations was that k_1 increases strongly with pressure at lower temperatures. Even though the negative temperature dependence[6−13] and pressure dependence[14,15] were known, the strong pressure dependence at low temperature was unmeasured, and extrapolation of the pressure dependence from higher temperatures underestimated k_1 at low temperatures.

Reaction 1 shows some unusual behavior. Above 300 K, k_1 exhibits only a weak temperature dependence and no measurable pressure dependence. At lower temperatures, the dependence on pressure increases markedly. Furthermore, the value of k_1 is quite small for a reaction that has a negative temperature dependence. The limited data available on the rate coefficient for the reaction of OD with DNO_3 show a very large kinetic isotope effect at 298 K ($k_H/k_D \sim 14$).[16] Furthermore, a significant pressure dependence for k(OD + DNO_3) was noted at 298 K but not at other temperatures. A complete understanding of the mechanism that gives rise to the unusual behavior of k_1 is interesting from a chemical kinetics point of view and is also an important step in verification of the temperature and pressure dependence under atmospheric conditions.

There have been a few attempts to elucidate the mechanism of reaction 1. Margitan and Watson,[14] and later Smith et al.,[11] showed that the observed pressure dependence requires the formation of an $OH{\cdot}HNO_3$ adduct that can undergo either dissociation back to OH and HNO_3 or react further to give products. Lamb et al.[17] and Marinelli and co-workers[10,18] worked on obtaining a mechanism consistent with the observations available to them. Marinelli and Johnston[10] explained the negative temperature dependence of k_1 by postulating a six membered ring transition state. Lamb et al.[17] suggested that a transition state in which OH attacks the N atom in HNO_3 best explained the observed temperature dependence.

This paper is a more detailed mechanistic study of reaction 1. We present measurements of rate coefficients for reactions between several different isotopomers.

$$OD + DNO_3 \rightarrow D_2O + NO_3 \qquad (2)$$

$$OD + HNO_3 \rightarrow HDO + NO_3 \qquad (3a)$$

$$\rightarrow OH + DNO_3 \qquad (3b)$$

$$OH + DNO_3 \rightarrow HDO + NO_3 \qquad (4a)$$

$$\rightarrow OD + HNO_3 \qquad (4b)$$

$$^{18}OH + HN^{16}O_3 \rightarrow H_2{}^{18}O + NO_3 \qquad (5a)$$

$$\rightarrow {}^{16}OH + HNO_3 \qquad (5b)$$

Measurement of the rate constants for reactions 2−5 explores

† Part of the special issue "Harold Johnston Festschrift".

‡ NOAA NRC Postdoctoral Fellow.

§ Also affiliated with: Cooperative Institute for Research in the Environmental Sciences, University of Colorado, Boulder, CO 80309.

|| Also affiliated with: Department of Chemistry and Biochemistry, University of Colorado, Boulder, CO 80309.

10.1021/jp002394m CCC: $20.00
Published on Web 12/30/2000

both the primary and secondary kinetic isotope effects arising from deuterium substitution on either HNO_3 or OH as well as the possibility for exchange reactions that might indicate the structure of any reactive complex and the barriers to reaction.

This paper also examines the question of the product yields from reaction 1. The reaction as written above is the most exothermic pathway, with $\Delta_r H°(298) = -17.3$ kcal mol^{-1}.[19] Production of hydrogen peroxide and NO_2 is also slightly exothermic,[19] although there is no direct experimental evidence for this pathway.

$$OH + HONO_2 \rightarrow H_2O_2 + NO_2 \qquad \Delta_r H°(298) = -1.8 \text{ kcal mol}^{-1} \quad (1b)$$

Wine et al.,[6] who first demonstrated the negative temperature dependence of k_1, suggested that the temperature dependence might in fact be due to reaction 1b. There have been several product yield studies of reaction 1.[8,9,18,20,21] Husain and Norrish[20] were the first to deduce H_2O and NO_3 as the products of reaction 1 on the basis of NO_3 absorption measurements. More recently, Ravishankara et al.,[9] Nelson et al.,[18] and Jourdain et al.[8] reported NO_3 as the only product, with a yield close to unity. Therefore, atmospheric modeling studies have assumed that reaction 1 leads only to $H_2O + NO_3$ products.

Further examination of the product yield is warranted for several reasons. First, it is important to atmospheric modeling since a significant yield for reaction 1b would impact calculations of HO_x abundance. Reaction 1 is a sink for HO_x; reaction 1b may or may not be a HO_x sink depending on the fate of H_2O_2 (i.e., further reaction with OH or photolysis). Second, there have been recent revisions and temperature dependence measurements of the recommended absorption cross-sections for NO_3 radicals[22] that were the basis for several of the previous yield studies. For example, Ravishankara et al.[9] reported an NO_3 yield of unity at both 298 and 251 K at fixed pressures of He and SF_6 bath gases; however, the upward revision of the NO_3 absorption cross-section suggests that the NO_3 yield from that study was in fact somewhat smaller than unity. Finally, there has been no explicit consideration of the pressure dependence of the product yield since the pressure dependence of k_1 was not widely appreciated at the time of the previous studies.

II. Experimental Section

Our previous study of reaction 1[1] describes the apparatus and the procedures that are important for accurate, low-temperature measurement of k_1. The first part of this section focuses on the additional details for measurement of rate constants for isotopically labeled species. The second part describes the apparatus and methods for measuring NO_3 yields.

A. Measurement of k_2-k_5. The experimental apparatus was a pulsed-photolysis, laser induced fluorescence (LIF) system. We produced OH (OD) radicals from a variety of photolytic precursors (described below) using a 248 nm KrF excimer laser, and we measured the temporal profile of OH (OD) after their photolytic production via pulsed LIF. The LIF light source (280−310 nm) was the frequency doubled output of a Nd:YAG laser pumped dye laser. All reactions took place under pseudo-first-order conditions, with $[OH]_0$ ($[OD]_0$) $< 10^{-3}[HNO_3]$ ($[DNO_3]$). The LIF/reaction cell was a jacketed Pyrex vessel with a volume of 150 cm^3. The linear gas flow velocity varied between 5 and 10 cm s^{-1} at all pressures, fast enough to refresh the gas mixture in the reaction zone every 1−2 laser shots in this 10 Hz experiment. Variation of the linear flow velocity had no effect on the measured rate constants. We calculated initial OH (OD) concentrations, $[OH]_0$ ($[OD]_0$), from the measured photolysis laser fluence and the known cross-sections of photolytic precursors (HNO_3,[23] O_3 [24]). We maintained $[OH]_0$ ($[OD]_0$) $\leq 4 \times 10^{11}$ cm^{-3} and checked that factor of 4 variation in photolysis laser fluence did not affect the measured rate constants. We measured the concentration of the HNO_3 (DNO_3) reactant via absorption (213.68 nm Zn line, $\sigma(HNO_3) = (4.52 \pm 0.19) \times 10^{-19}$ cm^2)[23] in either a 100 or 25 cm cell located either just downstream or upstream of the reactor. Comparison of ultraviolet spectra of HNO_3 and DNO_3 from this laboratory shows the DNO_3 cross-section at this wavelength to be within 10% of the HNO_3 cross-section. As described previously, we checked that there was no interference in the measured rate constants from the pressure dependent OH (OD) + NO_2 reaction[25] by measuring the NO_2 content of the HNO_3 (DNO_3) samples via LIF at 532 nm in an external cell. Our previous paper also described the synthesis and handling of anhydrous HNO_3 in detail.

Measurement of k_2, OD + DNO_3. Reaction 2 was the most straightforward of the isotopically labeled variants since the OD source was the 248 nm photolysis of the DNO_3 reactant. As discussed further below, reaction 2 is considerably slower than reaction 1, necessitating large concentrations of DNO_3 (3×10^{15} to 5×10^{16} cm^{-3}) to observe significant pseudo-first-order OD loss rate constants. We measured the DNO_3 concentration in a 25 cm external absorption cell, taking the 213.86 nm absorption cross-section for DNO_3 to be the same as that for HNO_3.

Measurement of k_3, OD + HNO_3. Measurement of k_3 was somewhat more difficult because the photolytic precursors for OD tend to undergo H/D exchange (most likely on surfaces) with the HNO_3 reactant, converting it partially into DNO_3 prior to generation of OD. We therefore used the reaction of $O(^1D)$, produced from 248 nm photolysis of O_3, with D_2 as the OD source since D_2 (unlike, for example, D_2O) does not exchange with HNO_3. This source avoided H/D exchange but could also regenerate OD via the following reaction sequence.

$$O(^1D) + HNO_3 \rightarrow OH + NO_3 \quad (6)$$

$$OH + D_2 \rightarrow HDO + D \quad (7)$$

$$OD + D_2 \rightarrow D_2O + D \quad (7b)$$

$$D + O_3 \rightarrow OD + O_2 \quad (8)$$

Reaction 7 is rather slow, having a value of $k_7 \approx 1.6 \times 10^{-15}$ cm^3 molecule^{-1} s^{-1} at 298 K,[26] and the contribution to the observed OD temporal profile can be minimized if the initial OH concentration is small. We measured the D_2 concentration in the reactor using calibrated mass flow meters, and then we simulated OD decays to include the effects of reactions (6−8).[2,27−29] For all reported measurements, $[O_3]$ was in the range $(1-2) \times 10^{14}$ molecules cm^{-3} and $[D_2]$ was in the range $(1.5-3.0) \times 10^{16}$ molecules cm^{-3}, although increasing $[D_2]$ by a factor of 5 did not affect measured rate constants. The corrections, estimated by numerical simulation of the reaction sequence, changed the k_3 values by 5% or less relative to those obtained without the correction.

Measurement of k_4, OH + DNO_3. The source chemistry for reaction 4 was the most difficult. The reaction of $O(^1D)$ with H_2 was not an optimal OH source in this case because the OH regeneration sequence that is analogous to reactions 7 and 8 contributed significantly to the OH temporal profile. The rate constant for OH + DNO_3 (k_4) is more than an order of magnitude smaller than k_3(OD + HNO_3), and the rate constant

for OH + H_2 is approximately four times faster than that for OD + D_2.[26] Thus, reaction 4 required an OH source that would neither exchange prior to reaction nor produce H atoms as byproducts. Therefore, we used the reaction of $O(^1D)$ with CF_3H as the OH source. Although the main reaction between these species is quenching of $O(^1D)$,[30,31] we found that O_3 photolysis in the presence of CF_3H did produce a sufficient amount of OH and that OH did not significantly react with the CF_3H precursor. The lack of a dependence of measured pseudo-first-order rate constants on the photolysis laser fluence showed that the $O(^3P)$ produced from quenching of $O(^1D)$ by CF_3H did not significantly participate in the reaction. Furthermore, as described further below, this source produces some OD from the reaction of $O(^1D)$ with DNO_3 and from DNO_3 photolysis, and we were able to simultaneously measure k_2 and k_4 by monitoring either OD or OH. The source accurately reproduced k_2(OD + DNO_3), further indicating that secondary chemistry was unimportant.

Measurement of k_5, $^{18}OH + HNO_3$. The reaction of $O(^1D)$ with $H_2{}^{18}O$ was a convenient and straightforward source for ^{18}OH. Since the O_3 that served as the $O(^1D)$ photolytic precursor was not isotopically labeled, the source produced approximately 50% each of ^{16}OH and ^{18}OH. We took advantage of the similar magnitude of LIF signals from both ^{16}OH and ^{18}OH, whose LIF transitions are adjacent to one another, to measure k_1 and k_5 directly in the same gas mixture. For each concentration of HNO_3 we measured the pseudo-first-order loss rate constant for ^{16}OH, then tuned the LIF probe laser wavelength to an ^{18}OH transition and measured the pseudo-first-order loss rate constant for that species.

B. NO_3 Product Yield. The NO_3 yield from reactions 1 and 2 was measured by producing OH (OD) radicals via pulsed laser photolysis in the presence of HNO_3 (DNO_3) and monitoring the temporal profile of NO_3 via absorption at 661.9 nm. The NO_3 yield for reaction 1 was measured between 20 and 770 Torr and at a few temperatures in the range 240−330 K. Reaction 2 was studied at room temperature over the pressure range 74−360 Torr. The apparatus, data acquisition, and procedures used to make such measurements have been described in recent work from this laboratory;[32,33] only a brief outline is given below.

Determination of the NO_3 product yield requires a quantitative measurement of the initial OH radical concentration, $[OH]_0$, and the NO_3 concentration produced by its reaction. Hydroxyl radicals were produced by the photolysis of HNO_3 at 248 nm (KrF excimer laser).

$$HNO_3 + h\nu \rightarrow OH + NO_2 \qquad (9)$$

The OH yield in reaction 9 has been measured to be unity.[34] Initial hydroxyl concentration, $[OH]_0$, was calculated from the excimer laser fluence and the measured HNO_3 concentration. The laser fluence was determined in separate calibration measurements using N_2O_5 photolysis at 248 nm

$$N_2O_5 + h\nu \rightarrow NO_2 + NO_3 \qquad (10)$$

and NO_3 transient absorption. The NO_3 yield in reaction 10 was taken as 0.8 in the present analysis.[2,35] The calibration was carried out using N_2O_5 because NO_3 could be measured in both the calibration and product yield studies. This reduced systematic error in the product yield determination associated with uncertainties in the wavelength used for monitoring NO_3 (diode laser) and the absorption cross-section of NO_3 at that wavelength.

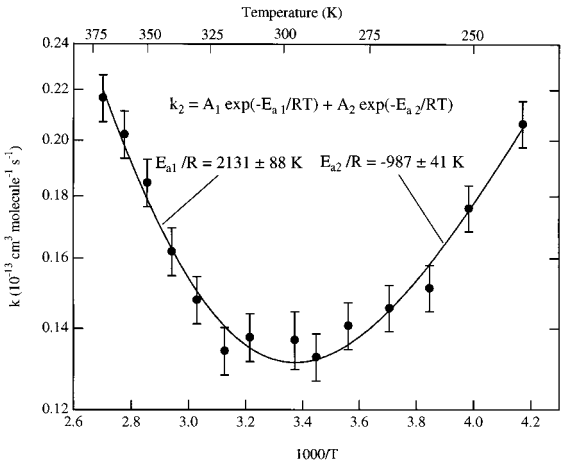

Figure 1. Variation of k_2 (OD + DNO_3) on a logarithmic scale vs $1/T$. The points are the values of k_2 measured in this work, and the solid line is the sum of two Arrhenius expressions using the E/R values indicated in the figure, and $A_1 = (5.52 \pm 0.09) \times 10^{-12}$ and $A_2 = (3.22 \pm 0.04) \times 10^{-16}$ cm^3 molecule^{-1} s^{-1}.

The apparatus consisted of a long-path absorption cell (path length of 91 cm), an excimer laser photolysis source (248 nm, KrF), and absorption light sources and detectors for measuring photolyte concentrations and monitoring the temporal evolution of NO_3. The jacketed absorption cell (30 mm i.d.) was made of Pyrex and was temperature regulated by circulating methanol from a controlled temperature bath through the jacket. A 662 nm diode laser, single mode with 0.5−2 mW output, was used to measure NO_3 transient absorption signals. The diode laser wavelength was locked at the peak of the NO_3 absorption feature, 661.9 nm, by regulating the laser current (∼40 mA) and temperature (∼275 K). The signal from the diode laser detector was sent to a multichannel scalar for digitization and signal averaging. Data acquisition was initiated approximately 1 ms before the excimer laser fired to provide a baseline from which changes in absorbance could be calculated. The NO_3 detection limit was $\sim 5 \times 10^9$ molecule cm^{-3} per laser shot.

Absorption by the photolytes were measured using a D_2 lamp (30 W) light source, a 0.5 m spectrograph, and a diode array detector. The spectrograph was equipped with a 300 grooves/mm grating and a 1024 element cooled diode array detector. The wavelength range of 200−365 nm was monitored. Concentrations of N_2O_5 and HNO_3 were determined using absorption cross-sections from the literature.[23,35] Wavelength calibration was made using emission lines from a Hg lamp and a 10 μm entrance slit.

All gases were mixed with the N_2 (UHP, 99.9995%) carrier gas prior to entering the absorption cell. Pressure was measured with a 1000 Torr capacitance manometer. The linear flow velocity of the gases in the absorption cell was normally 10 cm s^{-1}, leading to a transit time through the absorption cell of ∼10 s. The photolysis laser was operated either in single shot mode or below 0.1 Hz to ensure that a fresh gas mixture was available for each laser shot.

III. Results

A. Isotopically Substituted Reactions. Figure 1 presents our measurements of k_2, the rate constant for fully deuterated reactants, OD + DNO_3. Since both reactants are deuterated in this case, direct comparison of k_1 with k_2 includes both the primary (arising from D substitution on HNO_3) and secondary (D substitution on OH) kinetic isotope effects, but, as discussed further below, the primary kinetic isotope effect is by far the

TABLE 1: Measured OD + DNO_3 Rate Constants (k_2)[a]

T (K)	buffer gas	P (Torr)	k_2
	Pressure Dependence		
296	He	20.1	1.34 ± 0.08
		50.5	1.38 ± 0.10
		100.2	1.38 ± 0.07
		199.5	1.39 ± 0.08
	SF_6	50.0	1.22 ± 0.08
		100.3	1.22 ± 0.07
		201.1	1.47 ± 0.07
251	He	20.0	1.75 ± 0.09
		50.1	1.75 ± 0.08
		100.1	1.76 ± 0.08
		199.7	1.81 ± 0.10
	SF_6	50.0	1.64 ± 0.08
		100.1	1.62 ± 0.08
		199.7	1.75 ± 0.09
	Temperature Dependence		
370.1	He	100 ± 1	2.17 ± 0.10
360.2			2.02 ± 0.09
350.1			1.85 ± 0.08
340.0			1.62 ± 0.07
330.1			1.48 ± 0.07
319.9			1.34 ± 0.06
311.1			1.38 ± 0.06
296.5			1.37 ± 0.08
290.0			1.33 ± 0.06
280.8			1.41 ± 0.06
269.9			1.46 ± 0.06
260.0			1.51 ± 0.07
251.0			1.76 ± 0.08
239.7			2.07 ± 0.09

[a] The $[HNO_3]$ range is 3×10^{15} to 5×10^{16} molecules cm^{-3}. All rate constants in units of 10^{-14} cm^3 $molecule^{-1}$ s^{-1}, and the quoted uncertainties are $\pm 2\sigma$.

larger of the two. There are three salient features in Figure 1. The first is the vertical scale that ranges between 1.2×10^{-14} and 2.4×10^{-14} cm^3 $molecule^{-1}$ s^{-1}, anywhere between a factor of 5 and 50 times smaller than the rate constant for OH + HNO_3 over the same temperature range. The second is that Figure 1 is a plot of temperature dependence only; to within the 7% uncertainty of the measurement, k_2 lacks an observable pressure dependence over the range that we measured. Table 1 lists representative pressures over which k_2 was measured in both He and SF_6 buffer gases. Our result is in contrast to the study of Singleton and co-workers,[16,36] who found a somewhat unrealistic pressure dependence for k_2 of as much as 40% at room temperature but no pressure dependence at other temperatures. Thus, while we find a temperature dependence that is similar to the work of Singleton et al.,[16] we find no temperature between 240 and 370 K for which k_2 depends on pressure over the range 20−200 Torr of He and SF_6. This result is in marked contrast to reaction 1; at 250 K, k_1 increases by more than 50% over the same pressure and buffer gas range (see, for example, Figure 2). Finally, the most obvious feature of Figure 1 is the curvature in the temperature dependence, with a positive dependence at high temperature, a negative dependence at low temperature, and a minimum near 300 K. A fit to the sum of two separate Arrhenius expressions (solid line) describes the data in Figure 1, suggesting the presence of two competing reaction paths.

Reaction 3, OD + HNO_3, is a test of two different aspects of the reaction mechanism: the secondary kinetic isotope effect and the possibility for exchange, i.e., reaction 3b. Figure 2 is a plot of the pressure dependence of k_3 in He buffer gas compared to that for k_1 at 250, 296, and 350 K. (Also see Table 2.) Reaction 3 exhibits an essentially identical temperature and pressure dependence to reaction 1, but k_3 is consistently 10−30% larger than k_1 over the temperature and pressure ranges examined here.

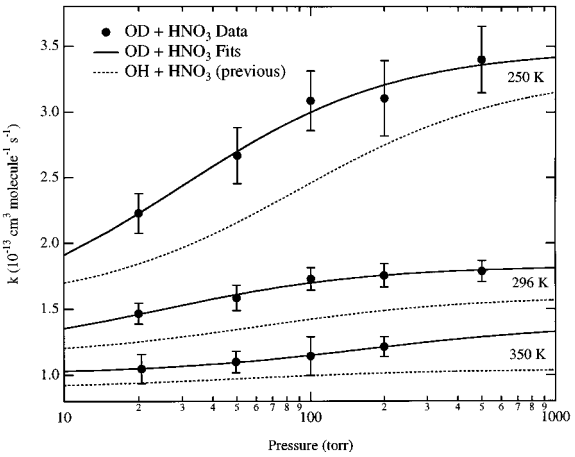

Figure 2. Pressure dependence for k_3 (OD + HNO_3) at three temperatures in He buffer gas. The solid points are the k_3 values from this work. The solid lines are fits to the pressure dependence for k_3 (OH + HNO_3) to the expression $k_0 + k_\Delta(1 + k_\Delta/k_c[M])^{-1}$, where k_0 is the bimolecular low-pressure limit, $k_0 + k_\Delta$ is the high-pressure limit, and k_c is a termolecular collisional relaxation rate constant. The dashed lines are the pressure dependences for k_1 (OH + HNO_3) in He, fit to the same form, from our previous study (ref 1).

TABLE 2: Measured Rate Constants for Reactions 3 and 4 in He Buffer Gas (Units of 10^{-13} cm^3 $molecule^{-1}$ s^{-1})[a]

T (K)	10^{15} [H(D)NO_3] (molecules cm^{-3})	P (Torr)	k
	k_3 (OD + HNO_3)		
250	0.4−6	20.0	2.23 ± 0.15
		50.2	2.67 ± 0.21
		100.2	3.09 ± 0.23
		200.5	3.10 ± 0.29
		498.8	3.40 ± 0.25
296	0.9−10	20.0	1.46 ± 0.08
		49.9	1.58 ± 0.10
		100.3	1.73 ± 0.09
		200.2	1.75 ± 0.09
		500.0	1.79 ± 0.08
350	1−14	20.5	1.05 ± 0.11
		49.6	1.10 ± 0.08
		100.0	1.14 ± 0.14
		200.0	1.21 ± 0.08
	k_4 (OH + DNO_3)		
297	2−50	100.3	0.108 ± 0.011

[a] Quoted uncertainties are $\pm 2\sigma$.

To ascertain if the increase in k_3 relative to k_1 was due to the contribution from the exchange, reaction 3b, we measured the temporal profile of OH during the course of the OD + HNO_3 reaction. As noted above, the photolytic OD source produces a small amount of OH from both the reaction of $O(^1D)$ with HNO_3 and from the 248 nm photolysis of HNO_3 itself. In the case of OD reacting with HNO_3 according to reactions 3a and 3b, and OH reacting according to reaction 1, the OH temporal profile is given by the following integrated rate expression.

$$[OH]_t = [OH]_0 \exp(-k_1' t) + [OD]_0 \frac{k_{3b}}{k_3 - k_1}[\exp(-k_1' t) - \exp(-k_3' t)] \quad (11)$$

Here, $k_1' = k_1[HNO_3] + k_d$, $k_3' = k_3[HNO_3] + k_d$, and k_d is the first-order rate coefficient for the loss of OH and OD out of the reaction zone due to diffusion and flow. Also, k_3 is the sum of k_{3a} and k_{3b}; $[OH]_0$ and $[OD]_0$ are initial concentrations. In 100

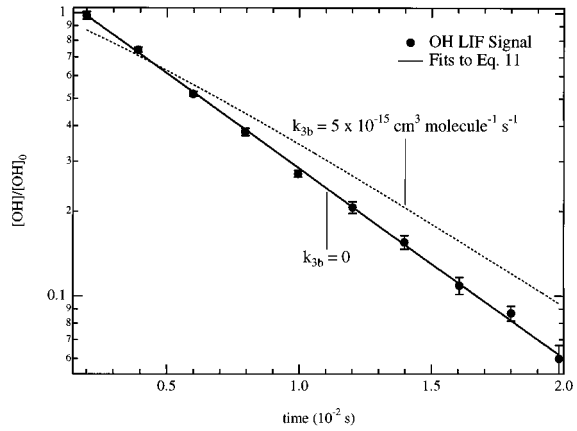

Figure 3. Temporal profile of OH (points) when OD is also produced in the presence of HNO_3. The solid and dashed lines are fits to eq 11 with k_{3b} set to zero and to a limiting value of 5×10^{-15} cm^3 molecule^{-1} s^{-1}, respectively. The calculated ratio of $[OD]_0/[OH]_0$ was 3.5 for the data shown in this figure.

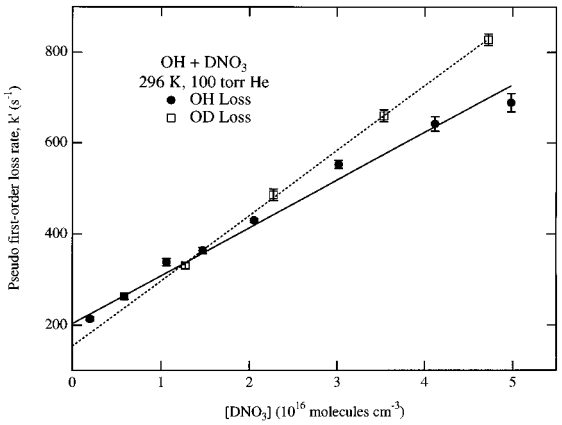

Figure 4. Plots of measured pseudo-first-order rate constants for loss of both OH (solid circles) and OD (open squares) as a function of DNO_3 concentration at 296 K and 100 Torr He. The slopes of linear least-squares fits (lines) to the data give the bimolecular rate constant for the two reactions.

Torr of He at 298 K, the measured difference between k_3 and k_1 is approximately 0.3×10^{-13} cm^3 molecule^{-1} s^{-1}. Measurement of pseudo-first-order OH loss rate constants as a function of $[HNO_3]$ in the presence of OD radicals reproduced (to within 5%) the previously measured value[1] for k_1 (100 Torr He, 296 K) of 1.40×10^{-13} cm^3 molecule^{-1} s^{-1}. Figure 3 demonstrates that a fit of the resulting OH temporal profiles to eq 11 sets an upper limit, $k_{3b} < 5 \times 10^{-15}$ cm^3 molecule^{-1} s^{-1}. The approximately 20% difference between k_3 and k_1 is therefore not due to a contribution from the exchange reaction. The increase in the rate constant upon deuteration of OH is due solely to the secondary kinetic isotope effect. (The term "secondary" means that the O−H(D) bond does not break in the reaction.)

Reaction 4 is similar to reaction 3 in that it is also a test for H/D exchange, i.e., reaction 4b. In this case, however, it is also a test of the primary, rather than secondary, kinetic isotope effect since the deuteration is on HNO_3. Because of the experimental difficulties noted above, we measured k_4 only at 296 K and 100 Torr He (see Table 2). Figure 4 shows the plot of the pseudo-first-order loss rate constants for both OH and OD as a function of DNO_3 concentration under identical pressure and temperature. We were able to measure both rate constants in the same reaction mixture as noted earlier. The slope of the fit to the OD data (dashed line) in Figure 4 gives a k_2 value consistent with that in Table 1 and Figure 1, while the slope of the fit to the OH data is approximately 20% smaller. The observation that OH reacts more slowly with DNO_3 than does OD and the lack of observable OD production at long reaction times strongly suggest that the exchange, reaction 4b, is not significant. Rather, the decrease in k_4 relative to k_2 is consistent with the secondary kinetic isotope effect described above; OH reacts slightly more slowly than does OD with either HNO_3 or DNO_3. One may surmise, in the absence of such measurements, that k_4 will have a pressure and temperature dependence similar to k_2 but have slightly smaller values.

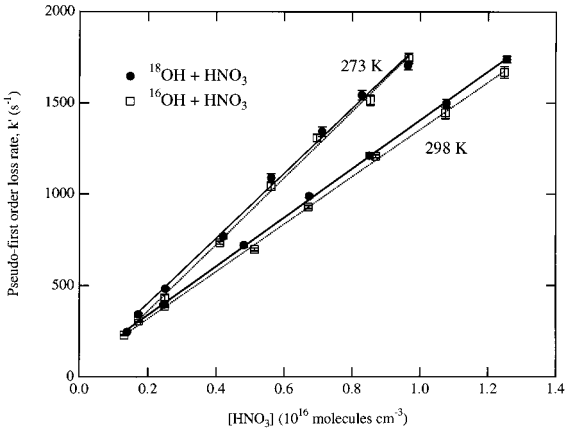

Figure 5. Pseudo-first-order rate constants for loss of ^{18}OH (solid circles) and ^{16}OH (open squares) vs HNO_3 concentration at two temperatures in 100 Torr He. The slopes of both data sets give the same rate constant to within the uncertainties of the linear least-squares fits at both temperatures. Solid lines are fits for ^{18}OH losses and dashed lines for ^{16}OH losses.

TABLE 3: Measured Rate Constants for Reaction 5 in He Buffer Gas (Units of 10^{-13} cm^3 molecule^{-1} s^{-1})

T (K)	10^{16} [HNO_3] (molecules cm^{-3})	P (Torr)	k_5 (^{18}OH+ HNO_3)	k_1 (^{16}OH + HNO_3)
295	0.13−1.3	99.6	1.33 ± 0.06	1.29 ± 0.08
273	0.17−1.0	100.4	1.78 ± 0.13	1.83 ± 0.12

We examined another exchange reaction, the $^{18}OH/^{16}OH$ exchange shown in reaction 5b. This experiment tests the suggestion, noted in the Introduction, that reaction 1 proceeds via a complex structure in which the hydroxyl O atom attacks the nitric acid N atom[17] (see Figure 10). One would expect a facile exchange between OH moieties in such a complex and thus facile $^{18}OH/^{16}OH$ exchange. Figure 5 displays plots of the measured pseudo-first-order rate constants for loss of ^{18}OH and ^{16}OH in the presence of HNO_3 in 100 Torr of He at 296 and 273 K. Clearly, the bimolecular rate constant for ^{16}OH and ^{18}OH reaction with HNO_3 are the same to within experimental uncertainty (see Table 3). Note that the derived values of k_1 agree with our previous data to within 9% at 296 K and 2% at 273 K. Thus, assuming that reaction 5a has the same rate constant as reaction 1, the rate constant for the exchange reaction in 5b is smaller than the experimental uncertainty in k_5, i.e., $<1 \times 10^{-14}$ cm^3 molecule^{-1} s^{-1}.

B. NO_3 Product Yields. To measure the NO_3 yield for reactions 1 and 2, it was necessary to first evaluate the excimer laser fluence by photolyzing N_2O_5 and measuring NO_3. The laser fluence is given by the following expression.

$$\text{laser fluence} = [NO_3]_{t=0}/([N_2O_5]_0 \sigma_{248\ nm}(N_2O_5)\ \Phi(NO_3)) \quad (12)$$

Here $[NO_3]_{t=0}$ is the NO_3 concentration produced by reaction 10 shortly after the photolysis pulse, $[N_2O_5]_0$ is the measured

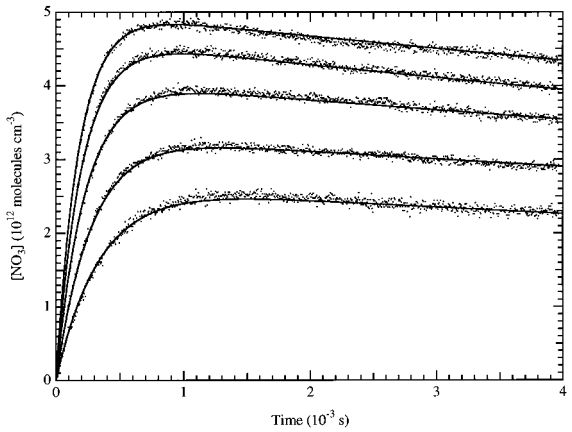

Figure 6. Measured temporal profiles (points) at 260 K and 300 Torr (N_2) of the NO_3 concentration arising from reaction 1 at five different HNO_3 concentrations. The solid lines are simulated profiles in which the NO_3 yield is the only variable (see text).

initial N_2O_5 concentration, $\sigma_{248\,nm}(N_2O_5)$ is the N_2O_5 cross-section at the photolysis wavelength, and $\Phi(NO_3)$ is the NO_3 yield in reaction 10. The precision of the laser fluence measurements was typically ~5% as determined from the slope of a plot of $[NO_3]_0$ vs $[N_2O_5]$. Calibration and product yield measurements were made in back to back measurements whenever possible. The laser fluence measured before and after the product yield experiments agreed to within the precision of the measurements. The NO_3 quantum yield from reaction 10 was observed to decrease slightly, but systematically, in going from 298 to 240 K (~3%) after accounting for the temperature dependences of the NO_3 and N_2O_5 absorption cross-sections. Although this effect was small, we calibrated the laser fluence at room temperature (i.e., photolyzed N_2O_5 at 298 K and then changed the temperature of the reactor) to minimize systematic errors in the measured product yields.

Figure 6 shows a representative set of NO_3 temporal profiles measured at 260 K and 300 Torr (N_2) upon generation of OH in the presence of HNO_3. The NO_3 profiles were typically measured at five different initial HNO_3 concentrations for each combination of temperature and pressure. Each trace in Figure 6 was obtained from a single excimer laser pulse. The temporal profiles of NO_3 gave the rate coefficients for OH loss. If the initial concentration of OH is known, then a comparison of NO_3 produced (after accounting for its slow loss) with $[OH]_0$ leads to the yield of NO_3 from reaction 1. However, there are small contributions to OH and NO_3 losses due to the following unavoidable side reactions.

$$OH + NO_2 + M \rightarrow HNO_3 + M \quad (13)$$

$$NO_2 + NO_3 + M \rightarrow N_2O_5 + M \quad (14)$$

$$OH + NO_3 \rightarrow HO_2 + NO_2 \quad (15)$$

Nitrogen dioxide is produced as a photolysis product in reaction 9 and is also present in small amounts (~100 ppmv) as an impurity in the HNO_3. The NO_3 profiles were numerically simulated for this set of reactions and fit to the observed profiles by varying only the yield of NO_3 in reaction 1. These calculated profiles are shown as solid lines in Figure 6. The rate coefficients for the simulations were taken from recent studies in this laboratory or DeMore et al.[2] Under the conditions of our measurements the secondary chemistry affects the NO_3 signal by less than 2%. As shown in Figure 6 the simulations reproduce the NO_3 profiles very well using our recently reported rate coefficient data for reaction 1[1] and NO_3 product yields near unity.

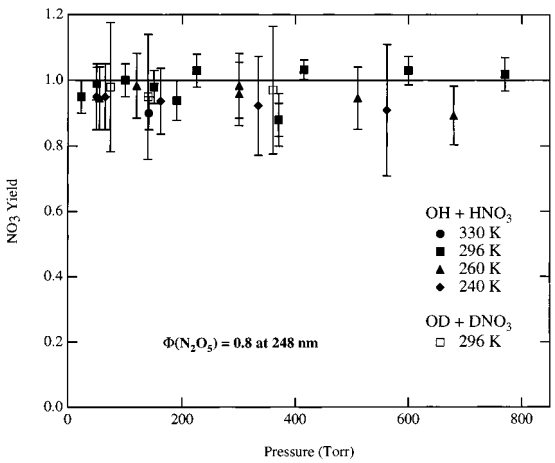

Figure 7. Measured NO_3 yield from reactions 1 and 2 for several temperatures (legend) as a function of pressure. To within experimental uncertainty, the yield does not vary with pressure and is unity at all temperatures.

TABLE 4: Measured Yields of NO_3 in the Reactions of OH with HNO_3 and OD with DNO_3 at Various Temperatures and Pressures (M = N_2)[a]

reaction	T (K)	P (Torr)	NO_3 yield ($\pm 1\sigma$)	no. of meaurements	$10^{16}[HNO_3]$ (molecules cm^{-3})
$OH + HNO_3$	330	370	0.88 ± 0.05	4	1.30−2.20
		141	0.90 ± 0.05	3	1.94−2.01
	296	770	1.02 ± 0.05	4	0.74−2.04
		600	1.03 ± 0.05	3	1.48−1.97
		415	1.03 ± 0.03	3	1.40−1.74
		190	0.94 ± 0.06	4	0.69−2.18
		50	0.99 ± 0.05	4	0.77−1.60
		100	1.00 ± 0.05	4	1.57−1.99
		150	0.98 ± 0.05	4	1.40−2.05
		225	1.03 ± 0.05	5	0.69−2.45
		370	0.88 ± 0.08	5	0.78−1.97
		23	0.95 ± 0.05	2	0.87, 1.52
	260	120	0.98 ± 0.05	5	0.88−2.40
		55	0.95 ± 0.025	4	1.08−1.77
		300	0.98 ± 0.02	5	1.08−2.05
		510	0.95 ± 0.02	3	1.44−1.59
		680	0.89 ± 0.01	3	1.84−2.57
		300	0.96 ± 0.03	6	1.09−2.47
	240	334	0.92 ± 0.15	2	0.86, 1.02
		562	0.91 ± 0.2	2	0.82, 0.87
		162	0.94 ± 0.1	2	0.97, 1.03
		65	0.95 ± 0.1	2	0.99, 1.06
		50	0.95 ± 0.1	2	1.00, 1.01
$OD + DNO_3$	296	74	0.98 ± 0.03	3	2.79−3.33
		140	0.95 ± 0.03	3	2.63−3.26
		360	0.97 ± 0.03	3	2.33−3.88

[a] The rate coefficients for the loss of the hydroxyl radical used in computing the yield were those determined in this study by following OH loss or from our previous study.[1]

The measured NO_3 yields as a function of pressure are summarized in Figure 7 and Table 4. Under the temperature and pressure conditions examined in this study, the NO_3 yield is near unity for both reactions 1 and 2. The largest uncertainty in this value originates from the uncertainty in the NO_3 quantum yield in reaction 10 which we estimate to be accurate to ±10%. We have taken a value of 0.8 for the above analysis. It should be noted that our absolute product yields are directly proportional to this value, but that our product measurements relative

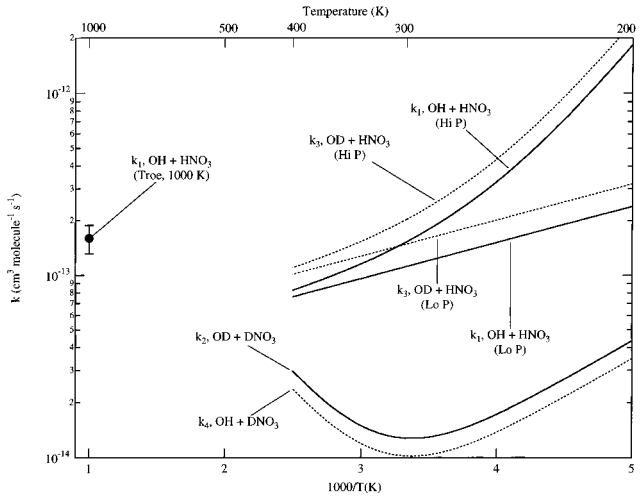

Figure 8. Overall variation of rate constants for reactions 1−4 with temperature and pressure. Reactions 1 (upper solid lines) and 3 (upper dashed lines) are both pressure dependent and have the same temperature dependence, except that k_3 is approximately 20% larger than k_1. A high-temperature value of k_1 from Troe[37] also appears as the solid point. Reaction 2 (lower solid line) is pressure independent and has a curved Arrhenius plot. We assume the same form for reaction 4 (lower dashed line), but with a 30% decrease in k_4 relative to k_2.

to each other (i.e., temperature and pressure dependence) are independent of the NO_3 yield from N_2O_5 photolysis.

Figure 7 demonstrates clearly that the NO_3 yields from reactions 1 and 2 do not vary with pressure or temperature, and that they are unity to within the uncertainty of this measurement. This result is not only important for atmospheric modeling, but it also shows that reactions 1−5 always give the same set of products irrespective of the various temperature and pressure dependences of their rate constants.

IV. Discussion

Figure 8 summarizes the temperature dependence of the rate constant data for reactions 1−4 in Arrhenius form. Fits from our previous study of reaction 1[1] (top solid lines) appear for both the high pressure and low-pressure behavior of the rate constant, and include a high-temperature measurement (solid point) from Troe.[37] The fit from the curved Arrhenius plot in Figure 1 appears as the lower solid line. The dashed lines represent the smaller magnitude of the secondary kinetic isotope effect, i.e., k_3 (upper) and k_4 (lower). Although we have not directly measured its temperature dependence, in Figure 8 we assume that k_4 (OH + DNO_3) has the same behavior as k_2 (OD + DNO_3).

A consistent picture of the mechanism for the reaction of OH with HNO_3 must explain the series of observations described in the results section and in Figure 8. First, below 300 K, k_1 displays a negative temperature dependence and a pressure dependence that increases with decreasing temperature. Second, any OH/OD or $^{16}OH/^{18}OH$ exchange reactions must be a factor of 10 (or more) slower than the reactions to form products. Third, the primary kinetic isotope effect (D substitution in HNO_3) decreases the rate constant by an order of magnitude, makes the rate constant pressure independent (over the 20−200 Torr range that we measured), and yields a markedly curved Arrhenius plot. Fourth, the secondary kinetic isotope effect (D substitution on OH) modestly increases the rate constant but does not significantly change the overall pressure and temperature dependence. Finally, reaction 1 yields only NO_3 and H_2O as products, irrespective of pressure and temperature. The

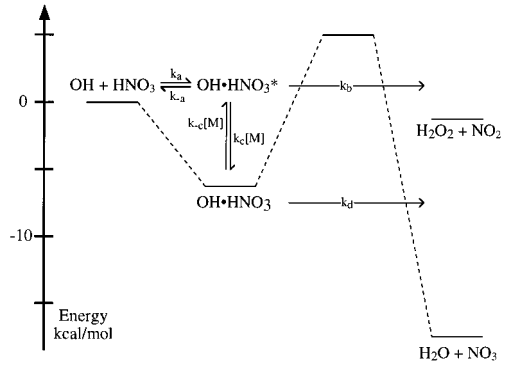

Figure 9. Proposed mechanism for reaction 1 showing adduct formation and subsequent reaction to form NO_3 and H_2O. Equation 16 in the text gives the overall rate constant that arises from the individual steps in the mechanism.

following discussion examines the implications of each of these observations in this order.

Previous studies of k_1 have established its negative temperature dependence and pressure dependence. Several studies have also suggested the general features of a reaction mechanism that includes a complex-forming step followed either by dissociation of the complex back to reactants or reaction from the complex to give products (see introduction). Figure 9 outlines such a mechanism. The kinetic scheme in the figure, combined with a steady-state approximation for the concentrations of the unrelaxed and relaxed intermediates, $OH{\cdot}HNO_3$* and $OH{\cdot}HNO_3$, yields the following expression for the overall rate constant.

$$k = k_a\left\{1 - k_{-a}\left(k_{-a} + k_b + \frac{k_d k_c[M]}{k_{-c}[M] + k_d}\right)^{-1}\right\} \quad (16)$$

This function gives a sigmoidal dependence on pressure. At both low and high pressures, eq 16 reaches bimolecular, pressure independent limits.

$$k_{LoP} = k_a\left(1 - \frac{k_{-a}}{k_{-a} + k_b}\right) = k_a\left(\frac{k_b}{k_{-a} + k_b}\right) \quad (17)$$

$$k_{HiP} = k_a\left(1 - \frac{k_{-a}}{k_{-a} + k_b + K_{eq}k_d}\right) = k_a\left(\frac{k_b + K_{eq}k_d}{k_{-a} + k_b + K_{eq}k_d}\right) \quad (18)$$

To arrive at eq 17, we have assumed $k_{-c}[M] \ll k_d$ and $k_c[M] \ll k_{-a} + k_b$, while in eq 18 we have assumed $k_{-c}[M] \gg k_d$. In eq 18, K_{eq} is the equilibrium constant between the energized and stabilized adduct, i.e., k_c/k_{-c}. We note that the pressure dependence in eq 16 has a behavior similar to that of the three-parameter function given by Lamb et al.[17] that we used in the analysis of our previous study[1] (see Figure 2). In reality, an $OH{\cdot}HNO_3$ adduct with energies anywhere between the fully thermalized state ($OH{\cdot}HNO_3$ in Figure 9) and the fully energized state ($OH{\cdot}HNO_3$* in Figure 9) will lead to products. Here, for the sake of simplicity, we have assumed a two state model. A full RRKM−master equation model is unlikely to give a different qualitative answer.

The observation that, at low temperature, k_1 has a finite value at low pressures but is pressure dependent over some intermediate range has two important implications in the context of the above model. First, the reaction barrier must be sufficiently large that redissociation of $OH{\cdot}HNO_3$* competes with reaction to products; i.e., k_{-a} cannot be negligible compared to k_b in eq

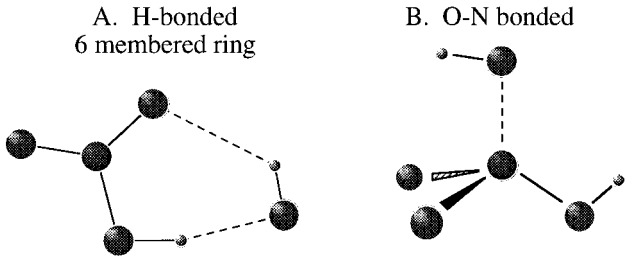

Figure 10. Two different proposed geometries for the adduct formed in the reaction of OH with HNO_3. Complex A is the doubly hydrogen-bonded, six membered ring. Complex B is the O−N bonded complex suggested by Lamb et al.[17]

16. If k_b were much greater than k_{-a}, the overall rate constant would be equal to the forward association rate constant, k_a, and would be independent of pressure. Second, formation of products from the stabilized adduct, $OH{\cdot}HNO_3$, must compete with collisional re-excitation that gives back reactants; i.e., $k_d \approx k_{-c}[M]$. If k_d is much less than $k_{-c}[M]$, the overall rate constant goes to the form of eq 18 and becomes pressure independent. Since formation of products from the adduct, either stabilized or unstabilized, clearly must proceed over at least a modest barrier, k_b and (particularly) k_d probably have a significant contribution from tunneling.

Figure 10 shows two plausible proposals for the structure of the $OH{\cdot}HNO_3$ adduct: complex A is a doubly hydrogen bonded, six membered ring,[10,14,15] and complex B is the one resulting from OH attachment to the N atom in HNO_3.[17] (The energy of the adduct shown in Figure 9 comes from ab initio calculations, as discussed further below.) Experimental observation of any of the exchange reaction 3b, 4b, or 5b, would have provided definitive evidence for the existence of one or both of the adducts in the figure. There is, however, no measurable exchange in either OH/OD or $^{16}OH/^{18}OH$ reaction. Thus, whatever the form of the complex, the barrier to the exchange reaction, either energetic or entropic, must be larger than that for reaction to form NO_3 and H_2O. If, as we argue, the adduct does form, the transition state leading to $NO_3 + H_2O$ must be smoothly connected to the complex. The path connecting complex A to this transition state would involve elongation of the $H-ONO_2$ bond. Starting from complex B, the transition state would require transfer of the nitric acid H to the hydroxyl O via a four-centered, tight transition state.

The O−N bonded complex structure (B in Figure 10) was favored by Lamb et al.[17] based on calculations showing that the Arrhenius behavior of k_1 for a tight transition state better matched the available data. Our results showing that $^{18}OH/^{16}OH$ exchange does not measurably occur suggests that reaction does not proceed through complex B, although this observation alone does not disprove this complex. Since the two OH groups are nearly identical in complex B, elimination of either to regenerate reactants should be facile, and one expects to observe both OH/OD and $^{16}OH/^{18}OH$ exchange.

Formation of the doubly hydrogen-bonded, six membered ring complex (A in Figure 10) appears to be a more plausible pathway. Indeed, recent ab initio calculations have predicted it to be bound by 6.0 kcal mol^{-1} with respect to OH and HNO_3.[38] This result is similar to the recent calculations of the nitric acid−water complex,[39] and agrees with other recent, unpublished, ab initio calculations.[40] Complex A is asymmetric, with a strong hydrogen bond between the H atom of nitric acid and the O atom of the hydroxyl, and a longer, somewhat weaker bond between the hydroxyl H atom and one of the nitric acid O atoms. The transition state for transfer of a single H atom from nitric acid to hydroxyl radical should have an asymmetric geometry, just as in complex A. By contrast, the transition state for the OH/OD exchange reaction should involve a symmetric (i.e., C_{2v} for the case of two H atoms) six membered ring that does not resemble the geometry of complex A. Thus, both the calculated geometry of the adduct and the experimental observations suggest that the barrier to the exchange reaction is larger than that for reaction to form NO_3 and H_2O.

The observation that deuteration of nitric acid dramatically reduces the rate constant, removes its pressure dependence, and results in the strongly curved Arrhenius plot of Figure 1 is consistent with the mechanism of Figure 9. The lack of pressure dependence comes from the balance between k_d and $k_{-c}[M]$ in eq 16. The first-order rate constants, k_b and k_d, are likely to be significantly slower for DNO_3 than for HNO_3 if tunneling is involved. Furthermore, the effective barrier height is slightly larger for the DNO_3 than for HNO_3 because of zero point energy stabilization of the reactants relative to the transition state, where one of the D atom motions has an imaginary frequency.[41] Deuterium substitution also increases the density of states in the adduct near the threshold for dissociation to reactants, leading to larger collisional rate constants, k_c and k_{-c}. Thus, it is plausible that for DNO_3, $k_{-c}[M] \gg k_d$ over the pressure range examined here, and that eq 18, which is independent of [M], is a good description of k_2 and k_4. Since both k_b and k_d are smaller for DNO_3 than for HNO_3, both will be quite small compared to k_{-a}. Therefore, k_2 and k_4 should have pressure independent rate constants that are much smaller than the high-pressure limits for k_1 or k_3, in accord with observations. Finally, the rate expression of eq 18 is consistent with the curved Arrhenius plot in Figure 1. Both k_b and $K_{eq}k_d$ will be much less than k_{-a}, so the overall rate constant from eq 18 will be proportional to their sum, $k_b + K_{eq}k_d$. The positive temperature dependence above 300 K in Figure 1 is most likely determined by k_b and gives a lower limit (because of tunneling) to the barrier height of $E_a \geq 4.3$ kcal mol^{-1}. The negative temperature dependence comes from K_{eq}, with the second term above dominant at lower temperature. It is noteworthy that the high-temperature measurement of k_1 ($OH + HNO_3$)[37] in Figure 8 shows that reaction 1 also has a positive temperature dependence at high enough temperatures, and should thus exhibit a curvature in its Arrhenius plot similar to that for k_2; this is a testable hypothesis. To our knowledge, there is no published value of a calculated barrier height for reaction 1.

The observation that deuteration of hydroxyl radical increases the rate constant only modestly is consistent with secondary kinetic isotope effects observed in other OH reactions, i.e., OH (OD) + H_2,[26] CH_4,[41] HCl,[42] etc. In these systems, the secondary kinetic isotope effect comes from the influence of zero point energy on the effective barrier height, particularly if the transition state has a bent geometry.

Finally, the fact that NO_3 is the only product of reaction 1 means that all of the observed dependences of the rate constant on temperature and pressure must be due to reactions producing a single set of products and not due to competition between pathways that give different products. Clearly, the above model qualitatively accounts for all observations without invoking any additional product channels. Furthermore, as Figure 11 demonstrates, eq 16 can reproduce the observed rate constants using reasonable values for k_a, k_{-a}, k_b, k_c, k_{-c}, and k_d. For example, one may estimate the forward association rate constant, k_a, based on the work of Smith and Williams,[43] who measured the quenching rate constant for $OH(v=1)$ by HNO_3 to be 2.5×10^{-11} cm^3 $molecule^{-1}$ s^{-1}. This quenching rate constant may

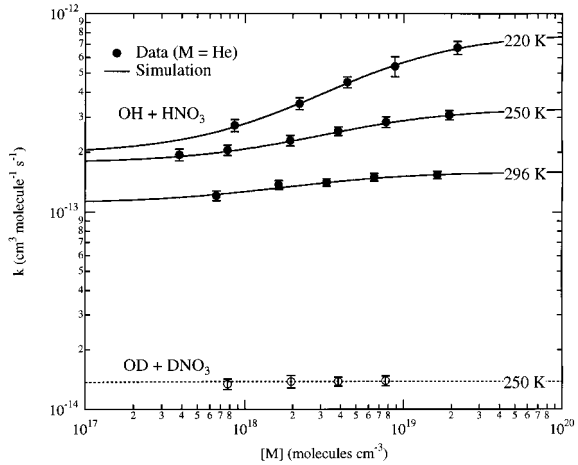

Figure 11. Variation of k_1 and k_2 with bath gas (He) number density (solid and open points, respectively). The solid and dashed lines are simulations of k_1 and k_2, respectively, using eq 16 and the rate constants in Table 4.

TABLE 5: Rate Constants Used To Simulate Experimental Data in Figure 11[a]

T (K)	k_c	k_b	k_d
	k_1 (OH + HNO_3)		
296	0.6	280	10
250	1.0	450	5.1
220	2.5	500	4.0
	k_2 (OD + DNO_3)		
250	1.0	33	0.025

[a] The values of k_a and k_{-a} are 1×10^{-11} cm^3 molecule^{-1} s^{-1} and 2.5×10^{10} s^{-1}, respectively, at all temperatures. k_c is in units of 10^{-10} cm^3 molecule^{-1} s^{-1}; k_b and k_d are in units of 10^6 s^{-1}.

have a contribution from resonant energy transer between OH-(v=1) and HNO_3, and we may thus assume $k_a \approx 1 \times 10^{-11}$ cm^3 molecule^{-1} s^{-1}. One may also estimate the value of the equilibrium constant, $K_{eq} = k_c/k_{-c}$, from the calculated OH·HNO_3 binding energy and the density of vibrational states in the well at the dissociation threshold. To count the vibrational state density, we used a Beyer−Swinehart algorithm[44] and the harmonic frequencies of Aloisio and Francisco.[38] These authors also give an equilibrium constant for the overall association reaction, OH + $HNO_3 \rightleftarrows$ OH·HNO_3. From their equilibrium constants, our calculated values for k_c/k_{-c} and the estimate for k_a, we estimate the first-order rate constant for dissociation of the energized complex back to reactants, k_{-a}, to be approximately 2.5×10^{10} s^{-1}. To simulate k_1 (solid lines in Figure 11), we used the above values for k_a and k_{-a} and, at each temperature, we adjusted k_b to match the observed low-pressure limit, k_d to match the observed high-pressure limit, and k_c to match the observed pressure dependence. Table 5 gives the k_c, k_b, and k_d values for three different temperatures. The unimolecular/tunneling rate constants, k_b and k_d, are reasonable, although the values for k_c are rather large. That the collisional relaxation must be so efficient in order to reproduce the observed pressure dependence indicates that the simple two-state model shown in Figure 9 (i.e., consideration only of OH·HNO_3* and OH·HNO_3) is probably inadequate. For example, collisional relaxation to states just below the dissociation threshold in the well will indeed be more efficient. Furthermore, formation of products via tunneling will occur from any vibrational state populated within the well.

To simulate the data for k_2 at 250 K (dashed line and open circles in Figure 11), we reduced the tunneling rate constant, k_d, by a factor of 200 relative to the simulation for k_1 at the same temperature. We estimated this factor by calculating the tunneling transmission probabilities for an asymmetric Eckart potential[45,46] with a barrier height relative to the bottom of the well of 11 kcal mol^{-1} (5 kcal mol^{-1} from separated reactants) and an exothermicity of −17 kcal mol^{-1} relative to reactants (−11 kcal mol^{-1} from the bottom of the adduct well). We used a characteristic length for the Eckart potential of 0.7 Å based on the calculated adduct geometry. We then adjusted k_b to match the observed rate constants (see Table 5). Clearly, reduction in the tunneling rate constant from the bottom of the well has the anticipated effect of removing the pressure dependence and dramatically reducing the overall rate constant. The lack of a pressure dependence is not sensitive to the value of k_d so long as it is at least a factor of 100 smaller than in the simulation of k_1 at the same temperature. Although it is too small to appear on the scale of Figure 11, there is a weak pressure dependence in the simulation of k_2, but it occurs only at pressures below the range of our measurement.

The model presented here is empirical and is not intended as a rigorous comparison of experiment to theory. It should, however, provide a framework for further experimental and theoretical study of reaction 1, and it does qualitatively account for all observations. As Figure 11 shows, our data, which lie mainly in the falloff region, may not accurately characterize either the high- or low-pressure limits of reaction 1, both of which would aid in a comparison between experiment and theory. Also, at low enough temperatures, there may be an observable pressure dependence for OD + DNO_3 that would be very sensitive to the value of the tunneling rate constant, k_d. Finally, this system should provide an excellent test of chemical kinetics theories in which tunneling plays an important role, particularly if a reliable potential energy surface connecting both reactants and products to the adduct can be calculated. Such a theoretical effort is currently underway.[40]

Acknowledgment. We thank Roberto Bianco and James T. (Casey) Hynes for many highly valuable discussions. Discussions with I. W. M. Smith, E. R. Lovejoy, and H. Stark were also very helpful. This work was funded in part by NASA's upper atmospheric research program. S.S.B. thanks the National Research Council for a postdoctoral fellowship.

References and Notes

(1) Brown, S. S.; Talukdar, R. K.; Ravishankara, A. R. *J. Phys. Chem.* **1999**, *103*, 3031.

(2) DeMore, W. B.; Sander, S. P.; Golden, D. M.; Hampson, R. F.; Kurylo, M. J.; Howard, C. J.; Ravishankara, A. R.; Kolb, C. E.; Molina, M. J. *Chemical Kinetics and Photochemical Data for Use in Stratospheric Modeling*; JPL Publication, 97-4; Jet Propulsion Laboratory: Pasadena, CA, 1997.

(3) Gao, R.-S.; Fahey, D. W.; DelNegro, L. A.; Donnelly, S. G.; Keim, E. R.; Neuman, J. A.; Teverovski, L.; Wennberg, P. O.; Hanisco, T. F.; Lazendorf, E. J.; Proffitt, M. H.; Margitan, J.; Wilson, J. C.; Elkins, J. W.; Stimpfle, R. M.; Cohen, R. C.; McElroy, C. T.; Bui, T. P.; Salawitch, R. J.; Brown, S. S.; Ravishankara, A. R.; Portmann, R. W.; Ko, M. K. W.; Weisenstein, D. K.; Newman, P. A. *Geophys. Res. Lett.* **1999**, *26*, 1153.

(4) Portmann, R. W.; Brown, S. S.; Gierczak, T.; Talukdar, R. K.; Burkholder, J. B.; Ravishankara, A. R. *Geophys. Res. Lett.* **1999**, *26*, 2387.

(5) Brühl, C.; Crutzen, P. J. *J. Geophys. Res.* **2000**, *105*, 12163.

(6) Wine, P. H.; Ravishankara, A. R.; Kruetter, N. M.; Shah, R. C.; Nicovich, J. M.; Thompson, R. L.; Wuebbles. *J. Geophys. Res.* **1981**, *86*, 1105.

(7) Kurylo, M. J.; Cornett, K. D.; Murphy, J. L. *J. Geophys. Res.* **1982**, *87*, 3081.

(8) Jourdain, J. L.; Poulet, G.; Le Bras, G. *J. Chem. Phys.* **1982**, *76*, 5827.

(9) Ravishankara, A. R.; Eisele, F. L.; Wine, P. H. *J. Phys. Chem.* **1982**, *86*, 1854.

(10) Marinelli, W. J.; Johnston, H. S. *J. Chem. Phys.* **1982**, *77*, 1225.

(11) Smith, C. A.; Molina, L. T.; Lamb, J. J.; Molina, M. J. *Int. J. Chem. Kinet.* **1984**, *16*, 41.
(12) Connell, P. S.; Howard, C. J. *Int. J. Chem. Kinet.* **1985**, *17*, 17.
(13) Devolder, P.; Carlier, M.; Pauwels, J. F.; Sochet, L. R. *Chem. Phys. Lett.* **1984**, *111*, 94.
(14) Margitan, J. J.; Watson, R. T. *J. Phys. Chem.* **1982**, *86*, 3819.
(15) Stachnik, R. A.; Molina, L. T.; Molina, M. J. *J. Phys. Chem.* **1985**, *90*, 2777.
(16) Singleton, D. L.; Paraskevopoulos, G.; Irwin, R. S. *J. Phys. Chem.* **1991**, *95*, 694.
(17) Lamb, J. J.; Mozurkewich, M.; Benson, S. W. *J. Phys. Chem.* **1984**, *88*, 6441.
(18) Nelson, H. H.; Marinelli, J.; Johnston, H. S. *Chem. Phys. Lett.* **1981**, *78*, 495.
(19) Atkinson, R.; Baulch, D. L.; Cox, R. A.; Hampson, R. F., Jr.; Kerr, J. A.; Rossi, M. J.; Troe, J. *J. Phys. Chem. Ref. Data* **1997**, *26*, 521.
(20) Husain, D.; Norrish, R. G. W. *Proc. R. Soc. London A* **1965**, *273*, 165.
(21) Glanzer, K.; Troe, J. *Ber. Bunsen-Ges. Phys. Chem.* **1974**, *78*, 71.
(22) Yokelson, R. J.; Burkholder, J. B.; Fox, R. W.; Talukdar, R. K.; Ravishankara, A. R. *J. Phys. Chem.* **1994**, *98*, 13144.
(23) Burkholder, J. B.; Talukdar, R. K.; Ravishankara, A. R.; Soloman, S. *J. Geophys. Res.* **1993**, *98*, 22, 937.
(24) Molina, L. T.; Molina, M. J. *J. Geophys. Res.* **1986**, *91*, 14501.
(25) Brown, S. S.; Talukdar, R. K.; Ravishankara, A. R. *Chem. Phys. Lett.* **1999**, *299*, 277.
(26) Talukdar, R. K.; Gierczak, T.; Goldfarb, L.; Rudich, Y.; Madhava Rao, B. S.; Ravishankara, A. R. *J. Phys. Chem.* **1996**, *100*, 3037.
(27) Yu, H. G.; Varanda, A. J. C. *J. Chem. Soc., Faraday Trans.* **1997**, *93*, 2651.
(28) Talukdar, R. K.; Ravishankara, A. R. *Chem. Phys. Lett.* **1996**, *253*, 177.
(29) Dunlea, E. Private communication.
(30) Force, A. P.; Wiesenfeld, J. R. *J. Phys. Chem.* **1981**, *85*, 782.
(31) Schmoltner, A. M.; Talukdar, R. K.; Warren, R. F.; Mellouki, A.; Goldfarb, L.; Gierczak, T.; McKeen, S. A.; Ravishankara, A. R. *J. Phys. Chem.* **1993**, *97*, 8976.
(32) Yokelson, R. J.; Burkholder, J. B.; Goldfarb, L.; Fox, R. W.; Gilles, M. K.; Ravishankara, A. R. *J. Phys. Chem.* **1995**, *99*, 13976.
(33) Yokelson, R. J.; Burkholder, J. B.; Fox, R. W.; Ravishankara, A. R. *J. Phys. Chem.* **1997**, *101*, 6667.
(34) Turnipseed, A. A.; Vaghjiani, G. H.; Thompson, J. E.; Ravishankara, A. R. *J. Chem. Phys.* **1992**, *96*, 5887.
(35) Harwood, M. H.; Burkholder, J. B.; Ravishankara, A. R. *J. Phys. Chem.* **1998**, *102*, 1309.
(36) Bossard, A. R.; Paraskevopoulos, G.; Singleton, D. L. *Chem. Phys. Lett.* **1987**, *134*, 583.
(37) Troe, J. *Ber. Bunsen-Ges. Phys. Chem.* **1974**, *78*, 74.
(38) Aloisio, S.; Francisco, J. S. *J. Phys. Chem. A* **1999**, *103*, 6049.
(39) Tao, F.-M.; Higgins, K.; Klemperer, W.; Nelson, D. D. *Geophys. Res. Lett.* **1996**, *23*, 1797.
(40) Bianco, R.; Hynes, J. T. Manuscript in preparation.
(41) Gierczak, T.; Talukdar, R. K.; Herdon, S. C.; Vaghjiani, G. L.; Ravishankara, A. R. *J. Phys. Chem.* **1997**, *101*, 3125.
(42) Battin-Leclerc, F.; Kim, I.; Talukdar, R. K.; Portmann, R. W.; Ravishankara, A. R.; Steckler, R.; Brown, D. *J. Phys. Chem.* **1999**, *103*, 3237.
(43) Smith, I. W. M.; Williams, M. D. *J. Chem. Soc., Faraday Trans. 2* **1985**, *81*, 1849.
(44) Gilbert, R. G.; Smith, S. C. *Theory of Unimolecular and Recombination Reactions*; Blackwell Scientific Publications: Oxford, U.K., 1990.
(45) Johnston, H. S.; Rapp, D. *J. Am. Chem. Soc.* **1961**, *83*, 1.
(46) Johnston, H. S.; Heicklen, J. *J. Phys. Chem.* **1962**, *66*, 532.